Determination of the iron oxidation state in Earth materials using XANES pre-edge information

Pierre-Emmanuel Petit[a], François Farges[b], Max Wilke[b] and V. Armando Solé[a]

[a]*European Synchrotron Radiation Facility, BP 220, F-38043 Grenoble Cedex, France*
[b]*Laboratoire des géomateriaux, Université de Marne-la-Vallée, F-77454 Marne la Vallée Cedex, France*
e-mail : ppetit@esrf.fr

Fe K-edge XANES spectra have been measured in more than 35 Fe(II) and Fe(III)-bearing minerals. The separation between the average pre-edge centroid positions for Fe(II) and Fe(III) is 1.4 ± 0.1 eV. Examination of calculated pre-edge features of mechanical mixtures of phases containing different proportions of Fe(II) and Fe(III) reveals that different trends of pre-edge position vs. pre-edge intensity can be observed, depending on the coordination environment. Both pre-edge parameters have been used to estimate the ferric/ferrous ratio in 12 natural minerals.

Keywords: iron, redox, minerals, XANES, pre-edge

1. Introduction

Iron is the most abundant transition element in Earth materials. The determination of its redox state is thus essential to constraint the thermodynamic conditions of formations of rocks and magmas (e.g., Parkinson & Arculus, 1997). XAFS spectroscopy is sensitive to the presence of these redox states, especially the pre-edge features (e.g., Waychunas *et al.*, 1983; Bajt *et al.*, 1994; Delaney *et al.*, 1998; Dyar *et al.*, 1998). As compared to the complementary L_2/L_3 edges of Fe (see Crocombette *et al.*, 1995), K-edges can be measured under extreme conditions or at the ppm level. We present the results of a Fe K-edge XANES spectroscopy study in a series of minerals, showing a wide range of environments around Fe, including trigonal bipyramids (which is common in Fe-bearing glasses: Brown *et al.*, 1995). We will also provide pre-edge information on mixtures between $^{[4]}$Fe(II), $^{[6]}$Fe(II), $^{[4]}$Fe(III), $^{[6]}$Fe(III), and test our method with 12 minerals.

2. Experimental

Fe K-edge XANES spectra were collected at the ESRF (Grenoble, France) on the undulator beamline ID26 (Gauthier *et al.*, 1999). The storage ring conditions were 6 GeV and 15-90 mA. A fixed-exit Si(220) double-crystal monochromator was used, providing an energy resolution of ~ 0.4 eV at the Fe K-edge, which is much less than the Fe-K natural line width (~ 1.15 eV: Krause & Oliver, 1979). For all spectra, a metallic Fe reference foil was used to provide an energy calibration for the monochromator (energy reproducibility: ± 0.05 eV). We used two Si mirrors for the harmonics rejection. XAFS data for most model compounds were collected in transmission and fluorescence mode simultaneously with Si photodiodes, using the geometry described by Tröger *et al.* (1992) to minimize self-absorption effects in XAFS fluorescence spectra (at lower Fe concentration, the sample was positioned 45° with respect to the beam). We used powdered samples.

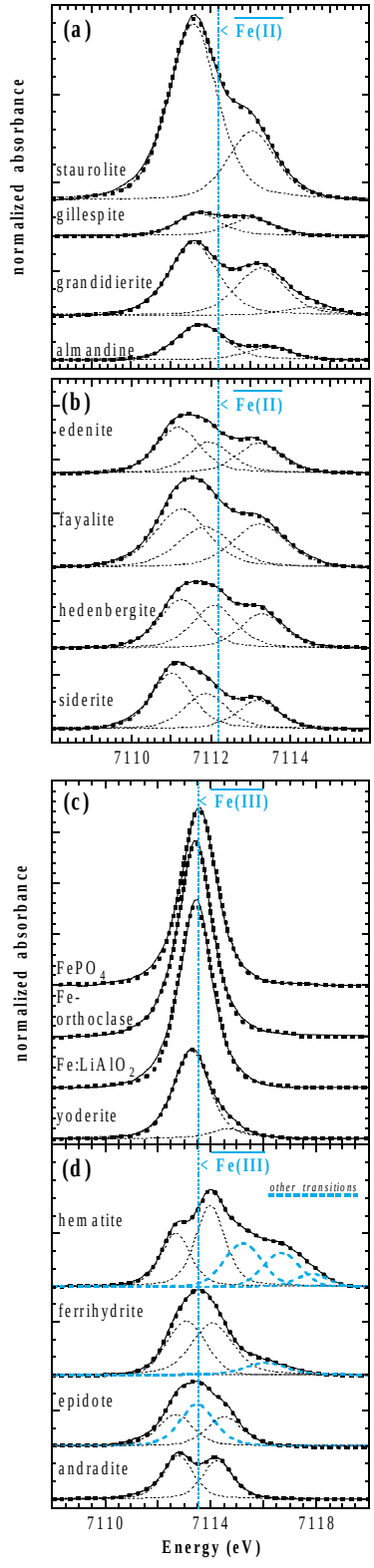

Figure 1
Selected normalized pre-edge spectra (Fe K-edge) and the best model calculated; (a) pre-edges for 4-, 5-, and 8-coordinated Fe(II) model compounds; (b) pre-edges for 6-coordinated Fe(II) model compounds; (c) pre-edges for 4- and 5-coordinated Fe(III) model compounds; (d) pre-edges for 6-coordinated Fe(III) model compounds showing extra transitions (in gray dotted lines) related to some Fe clustering (epidote, ferrihydrite, and hematite).

The XANES spectra were normalized by using a Victoreen function to subtract the background absorption and an arctangent function to normalize the height of the edge jump. The contribution of the edge jump to the pre-edge feature was modeled using an interpolation function (spline function). The pre-edge features were then fit into pseudo-Voigt components, by fixing the Gaussian fraction to 50 % and assuming the same width for each pre-edge feature, which was found to be ~1.4 eV. From the parameters of the fit, we calculated the "total integrated area" (sum of the integrated areas of each component) and the centroid (area-weighted average of the positions of each component).

3. Results

3.1. Ferrous model compounds

When iron is located in a tetrahedral site, which is the case for staurolite (Fig. 1a), hercynite and chromite, the pre-edge features may be decomposed into two components. For 5-coordinated Fe(II) with trigonal bipyramid geometry (as in grandidierite), a third component could be fit (Fig. 1a), which is due to the presence of Fe(III) (see below). In gillespite (square planar (D_{4h}) symmetry), the pre-edge feature can be modeled with two components (Fig. 1a), which is also the case when Fe(II) is located 8- (almandine) or 12-coordinated site (silicate perovskite). For octahedral Fe(II) model compounds (Fig. 1b), a third component is distinguishable in the raw pre-edge data when the octahedron is regular around Fe (O_h symmetry), which is the case for siderite or ferrous sulphate**.** All spectra must be modeled with three components. For all ferrous model compounds, the average centroid of the pre-edge is near 7112.1(1) eV (Fig. 2). The samples of wüstite and magnesiowüstite have always a small amount of Fe(III) (e.g., Waychunas, 1983), which explains their relatively high values. As pointed out previously (e.g., Waychunas *et al.*, 1983; Westre *et al.*, 1988), the pre-edge features are much less intense when the site of iron is centrosymmetric (O_h and D_{4h} symmetries), and the most intense pre-edge structures are observed for the most non-centrosymmetric geometry (Fig. 2).

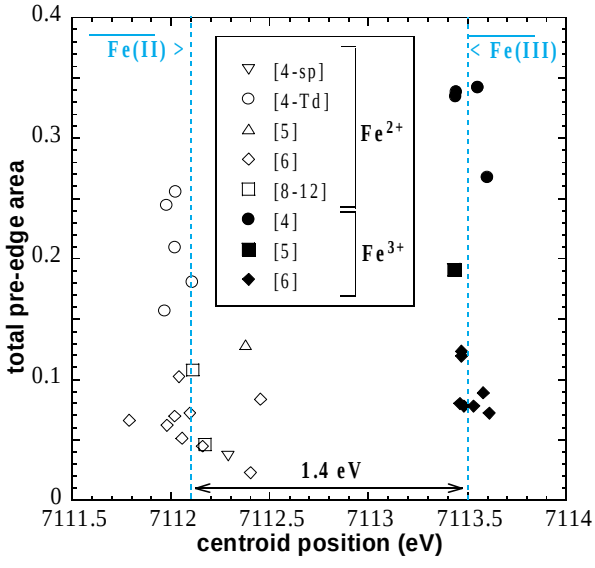

Figure 2
Summary of pre-edge characteristics, showing the separation between Fe(II) and Fe(III) centroids. The relatively large deviation for grandidierite (tip up triangles), gillespite (tip down triangles), and Fe(II)-oxides are due to some minor amounts of Fe(III) in these samples.

3.2. Ferric model compounds

The same trends as for ferrous compounds are observed (Fig. 2), but with some differences. The centroid of the pre-edge features is located at around 7113.5(1) eV. In a tetrahedral environment, we can observe one intense peak, which we modeled with a single contribution (Fig. 1c). For yoderite (Fe(III) in a trigonal bipyramid), the pre-edge structure, less intense, has to be fit with two contributions (Fig. 1c). For compounds with octahedrally coordinated Fe(III), the pre-edge intensity decreases. In several compounds, as andradite (Fig. 1d), titanomelanite and ferric sulfate, two components are observed in the pre-edge spectra. In hematite, goethite, and ferrihydrite, however, one to three extra components are observed in the pre-edge features above 7115 eV (Fig. 1d). Polarization-dependent XAFS experiments on hematite suggest that these contributions are related to long-range order, including Fe-Fe pairs (Dräger *et al.*, 1988). Also, their intensity increases with the degree of Fe-octahedral polymerization (ferrihydrite < goethite < hematite). These contributions have thus been excluded for the calculation of the pre-edge centroid and the total integrated area, which are then in agreement with those of the other Fe(III) model compounds. The same argument can be applied to epidote.

4. Discussion

The centroids for ferrous and ferric iron are separated by 1.4(1) eV (Fig. 3), in agreement with past studies (Waychunas *et al.*, 1983; Bajt *et al.*, 1994; Galoisy & Calas, 2000). To check if it is possible to derive accurate ferrous/ferric ratio from the pre-edge parameters, we have calculated the pre-edge spectra for 6 possible binary mixtures between four phases (staurolite, siderite, $FePO_4$ and hematite), containing $^{[4]}$Fe(II), $^{[6]}$Fe(II), $^{[4]}$Fe(III), and $^{[6]}$Fe(III) (we consider mixtures made on a molar basis with respect to the Fe atom in the compound). From the calculated pre-edge spectra, we have derived the values of the pre-edge parameters (Fig. 3). Slightly non linear variations for $^{[4]}$Fe(II)-$^{[4]}$Fe(III) and $^{[6]}$Fe(II)-$^{[6]}$Fe(III) mixtures are obtained. The most non-linear variations are observed when both the oxidation state and the coordination number of Fe vary simultaneously.

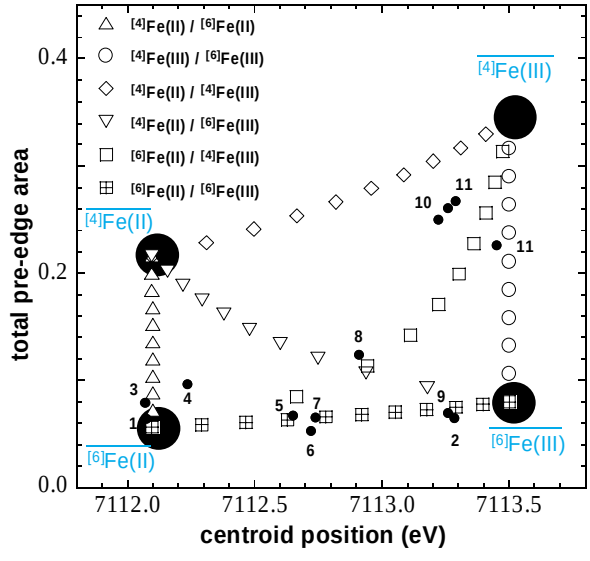

Figure 3
Summary of pre-edge characteristics for the binary mixtures between $^{[4]}$Fe(II), $^{[6]}$Fe(II), $^{[4]}$Fe(III), and $^{[6]}$Fe(III). In addition, pre-edge information for Fe in example minerals is also plotted. Black circles are: 1 humite; 2 rhodonite #1; 3 rhodonite #2; 4 dumortierite; 5 potassian kaersutite; 6 kaersutite; 7 vesuvianite #1; 8 vesuvianite #2; 9 franklinite, 10 magnetite #1 & #2; 11 labradorite; 12 maghemite.

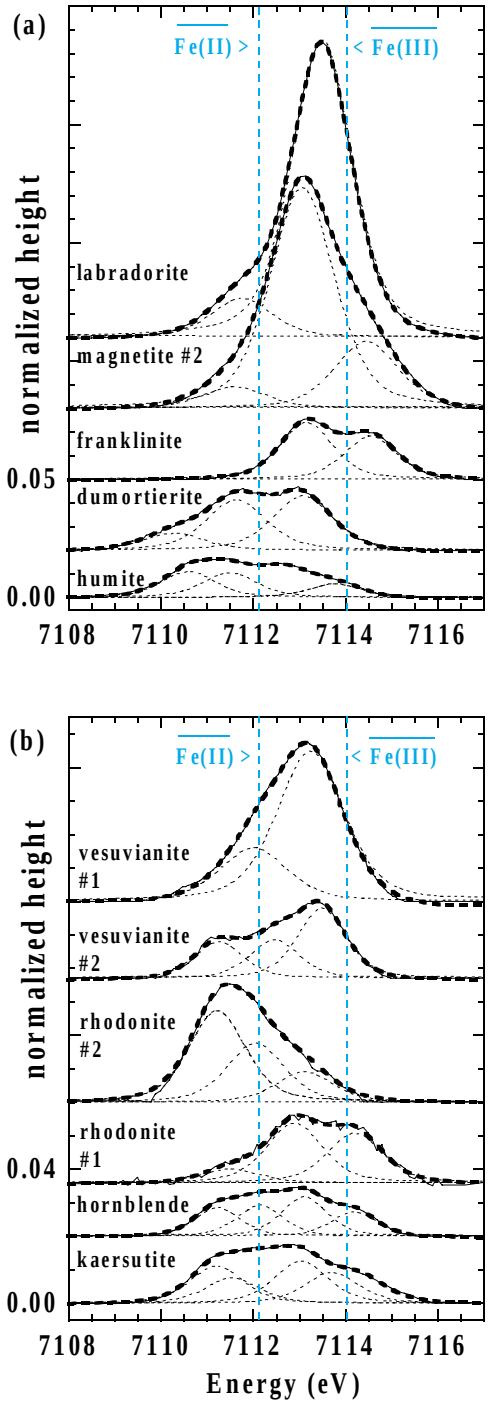

Figure 4
Fe K-edge pre-edge feature for the minerals used to evaluate their Fe oxidation states.

We will now use this diagram to analyze Fe oxidation state in several crystals. Magnetite has an inverse spinel structure, and there are contributions of $^{[6]}$Fe(III), $^{[4]}$Fe(III), and $^{[6]}$Fe(II) in its pre-edge structure (Fig. 4a). Fig. 3 leads to estimate an amount of 60-70 % of ferric iron, which is consistent with the actual redox state. Franklinite (Fig. 4a) has a spinel structure, and its pre-edge parameters are located close to the $^{[6]}$Fe(III) end-member (Fig. 3), with an amount of ~90%. The Fe-bearing labradorite (Fig. 4a) has a pre-edge feature close to that of Fe-orthoclase. Fig. 3 suggests that there is an amount of 70-80% of Fe(III) in that sample, in agreement with other ferrous/ferric determinations (Hofmeister & Rossman, 1983). Humite and dumortierite have pre-edges structures (Fig. 4b) dominated by the presence of $^{[6]}$Fe(II), which is consistent with their crystal structures (Alexander *et al.*, 1986). The pre-edges structures of the two amphiboles, ferrihornblende and kaersutite, may be modeled by considering 2+2 contributions (Fig. 4b), typical of octahedral ferrous and ferric iron. Both spectra are almost the same, but the component peaks are quite different: here, the fits are probably not unique. The pre-edge features of the two samples of rhodonites are typical of octahedral iron (Fig. 4b). The sample rhodonite#1 is rich in ferric iron (80 % based on Fig. 3), whereas the sample rhodonite#2 present more than 90 % $^{[6]}$Fe(II). In vesuvianite, iron may be found in two sites (Ohkawa *et al.*, 1992): $^{[5]}$Fe (square pyramidal geometry) and $^{[6]}$Fe. In Fig. 3, vesuvianite#1 is located on the $^{[6]}$Fe(II)/$^{[6]}$Fe(III) join, which excludes the presence of $^{[5]}$Fe, whereas the pre-edge parameters of vesuvianite#2 do not exclude this possibility.

In conclusion, we have seen that it is possible to derive iron redox information from the centroid of the pre-edge position if the influence of Fe-coordination is taken into account. In glasses and melts, Fe may be distributed over 4 distinct site geometries (Brown *et al.*, 1995). This requires a thorough analysis of the pre-edge structures. Collection of high resolution spectra, such as on an undulator beamline, is a key to derive significantly more robust information.

This work was supported by the EEC TMR network “Water in Molten Silicates” (FF). We thank Gordon E. Brown Jr., Glenn A. Waychunas, Jean-Claude Boulliard, Stéphanie Rossano, Yanbin Wang, L. Bonneviot and I. Berrodier for providing some of the specimens used in this study

References

Alexander, V. D., Griffen, D. T., & Martin, T. J. (1986) *Am. Mineral.*, **71**, 786-794.
Bajt, S., Sutton S.R., & Delaney, J. S. (1994) *Geochim. Cosmochim. Acta* **58**, 5209-5214
Brown, G. E., Jr., Farges, F., & Calas, G. (1995) In *Structure, Dynamics, and Properties of Silicate Melts* (eds.. J. F. Stebbins, D. B. Dingwell, & P. F. McMillan), pp. 317-410, *Reviews in Mineralogy*, Vol. **32**, The Mineralogical Society of America, Washington, DC.
Crocombette, J.P., Pollack, M., Jollet, F., Thromat, N., & Gautier-Soyer, M. (1995) *Phys. Rev. B*, **52**, 3143-3150
Delaney J.S., Dyar M.D, Sutton, S.R., & Bajt S. (1998) *Geology*, **26**, 139-142
Dräger, G., Frahm, R., Materlik, G., & Brummer, O. (1988) *Phys. Stat. Sol. B*, **146**, 287-293.
Dyar, M.D., Delaney, J.S., Sutton, S.R., & Schaefer, M.W. (1998) *Am. Mineral.* **83**, 1361-1365
Galoisy, L., & Calas, G. (2000) (*submitted*).
Gauthier, C., Solé, V. A., Signorato, R., Goulon, J., & Moguiline, E. (1999) *J. Synchrotron Rad.*, **6**, 164-166.
Hofmeister, A. M., & Rossman, G. R. (1984) *Phys. Chem. Minerals*, **11**, 213-224.
Krause, M.O., & Oliver, J.H. (1979) *J. Phys. Chem. Ref. Data*, **8**,329-338
Ohkawa, M., Yoshiasa, A., & Takeno, S. (1992) *Am. Mineral.*, 77, 945-953.
Parkinson, I. J., & Arculus, R. J. (1997) *Chem. Geol.*, **160**, 409-423.
Tröger, L., Arvanitis, D., Baberschke, K., Michaelis, H., Grimm, U., & Zschech, E. (1992) *Phys. Rev. B*, **46**, 3283-3289.
Waychunas, G. A. (1983) *J. Mat. Science*, **18**, 195-207.
Waychunas, G. A., Brown, G.E. Jr., & Apted, M. J. (1983) *Phys. Chem. Minerals*, **10**, 1-9.
Westre, T.E., Kennepohl, P., de Witt, J., Hedman, B., Hodgson, K.O., & Solomon, E.I. (1997) *J. Am. Chem. Soc.*, 119, 6297-6314.